CHALMERS

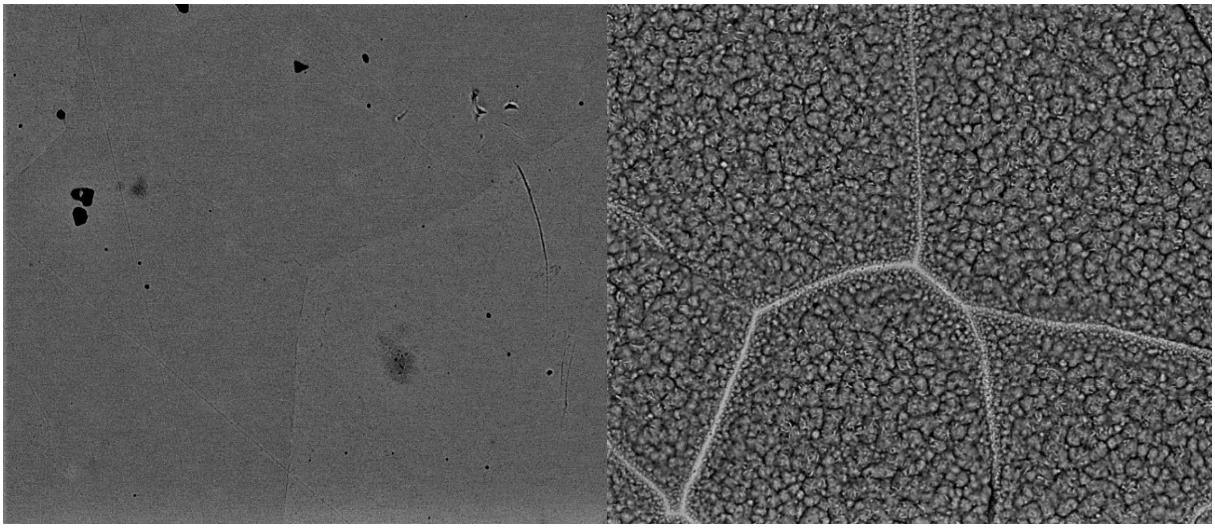

The influence of Ni on corrosion of Fe-18Cr model alloys at 600°C

- A mass-gain study

Degree project in the bachelor program of chemical engineering

FANNY KARLSSON

DEPARTMENT OF CHEMISTRY AND CHEMICAL ENGINEERING
CHALMERS UNIVERSITY OF TECHNOLOGY
Gothenburg, Sweden 2019

The influence of Ni on corrosion of Fe-18Cr model alloys at 600°C
A mass-gain study
FANNY KARLSSON

© FANNY KARLSSON, 2019

Supervisor: Amanda Persdotter, Johan Eklund & Torbjörn Jonsson, Department of Chemistry and Chemical Engineering.

Examiner: Lars-Gunnar Johansson

Degree project 2019

Department of Chemistry and Chemical Engineering

Division of High Temperature Corrosion

Chalmers University of Technology

SE-412 96 Gothenburg

Telephone +46 31 772 1000

Cover: Plan-view SEM images of the alloy without nickel added and the one with the highest nickel content in this study.

Printed by Chalmers Reproservice

Gothenburg, Sweden 2020

Abstract

Stainless steels are extensively used materials with corrosion resistant properties assigned to the formation of the chromium rich corundum type oxide that forms. However, as the primary protection are damaged stainless steel can suffer from breakaway corrosion which may happen if introducing K_2CO_3. In addition to chromium, nickel plays a significant role in the aspect of corrosion resistance since it promotes face-centred cubic structure which improves preferable properties such as it becomes less brittle and the formability as well as the weldability improves. Besides, nickel addition compensates for the loss of toughness that results when adding chromium. One disadvantage with using nickel is that it is expensive, making it interesting to investigate whether higher levels of nickel is necessary.

This present work focuses on how mass-gain changes as the nickel content increases. A set of Fe18Cr- model alloys with varying nickel addition between 0-82wt% were examined. All samples were exposed for 168 h in 600℃ in dry condition (5% O_2, bal. N_2) in a horizontal tube furnace. SEM and EDX analyses were performed on all alloys. Results were compared with a study limited to examine the secondary protection where 1 mg/cm^2 K_2CO_3 were sprayed on all samples but exposed under the same conditions as in this work. Another study made on the same set of alloys, known as TEAMWORK, exposed the samples for 24 h resulting in comparison focused on the effect of exposure time.

As the nickel content reached 20wt% mass-gain increased notably and reached its highest for the alloy containing 34wt% Ni indicating that the stainless properties were lost. Looking at the results from this work along with the related studies indicate that the amount of nickel necessary to maintain the stainless corrosion properties differs depending on if the material is in the primary or secondary corrosion regime.

Keywords: Fe18Cr-alloys, Nickel, primary protection, horizontal tube furnace, mass-gain.

Content

11 Introduction 6
1.1 Background 6
1.2 Aim 7
1.3 Limitations 7
2 Materials 8
2.1 Stainless steel 8
2.2 Alloying elements 8
3 Oxidation of Metals 10
3.1 Thermodynamics 10
3.2 Oxide formation 11
3.3 Oxidation kinetics 14
3.3.1 Linear rate law 14
3.3.2 Parabolic rate law 15
3.3.3 Logarithmic rate law 15
3.3.4 Breakaway oxidation 15
4 Corrosion Products 16
4.1 Chromium oxides 16
4.2 Iron oxides 16
4.3 Nickel oxides 17
5 Experimental Procedure 18
5.1 Investigated materials 18
5.2 Sample preparation 19
5.3 Furnace exposure 19
5.4 Calculation of oxide thickness 20
6 Analytical Techniques 21
6.1 Scanning electron microscopy (SEM) 21
6.2 Energy Dispersive X-ray Spectroscopy (EDX) 21
7 Results 22
7.1 Influence of nickel 22
7.1.1 Mass-gain and oxide thickness 22
7.1.2 Analytical results 24
8 Discussion 28
9 Future work 29

1
Introduction

Metal alloys are used in a wide range of applications in various environmental conditions, yet all suffer from corrosion affecting the alloys negatively. For high temperature applications the usage of alloying elements such as chromium and nickel are of great importance for iron-based alloys. These elements are added with purpose of improving its mechanical properties as well as the corrosion resistance, and small adjustments in the composition can have major influence. The corrosion resistance is primarily assigned to the ability to form protective chromium rich corundum type oxide scales and the material group is commonly referred to as chromia forming alloys. The protective oxide layers act as a diffusion barrier between the metal and the oxidizing environment, slowing down the oxidation rate. In relatively mild environments these oxide scales act protective, designating the primary protection. However, as the environment turns harsher the protective oxide scales may break down by depletion of chromium, causing so-called breakaway corrosion. The breakdown of the chromium rich oxide will result in the formation of a less protective iron rich oxide, referred to as the secondary protection. The secondary protection of so called chromia forming alloys has not been investigated in the same extent as the primary protection and the influence of different alloying elements for the secondary protection behaviour is not very well understood. Since nickel is an expensive alloying element it is of interest to investigate whether high levels are necessary from a corrosion perspective. An increased understanding of how the primary protection is affected by addition of nickel at mild conditions, compared to how the same alloys behave in harsher environments is necessary to gain an overall understanding of what influence that the commonly used alloying element has. This is why this study is focused on investigating the influence of nickel, on the primary protection of mainly Fe-18Cr alloys. The results will be later compared to the secondary protection behaviour.

1.1 Background

Nickel consisting alloys are often found in food contact materials, process powerplants and architecture due to the ease of cleaning, maintenance of hygiene as well as for its overall strength and contribution to the corrosion resistance. Approximately 75% of the stainless steel grades produced consists of nickel as a consequence for decreased toughness caused by chromium addition, nickel is added to compensate.(1) The Nickel Institute claims that even though chromium is the element contributing with the “stainless”-properties it is the additional nickel that enables stainless steel to become such a versatile alloy. This results from the fact that nickel in addition to its inherent corrosion resistance are easy to form and weld, they remain ductile at low temperatures and yet are useful for high temperature applications. For example, nickel-based super alloys play a vital role in engineering applications at high temperatures. The development of these alloys involves additional chromium, aluminium, cobolt, molybdenum, iron along others to achieve high strength and better oxidation and corrosion resistance. Turbine components facing aggressive corrosion environments are typically made of nickel-based super alloys. (2)

A great amount of previous studies has been made focusing on the influence that different alloying element has, but also how different materials behave in various environments. These are often executed in presence of either water vapour and/or Cl-ions, but also in milder

conditions, e.g. dry 5%O_2, as a reference. For 304L in environments with water vapour + O_2 chromium evaporation can occur, which is indicated by a mass-loss. In comparison, dry condition exposures result in mass-gain and chromium rich oxide formation. (3) For Sanicro 28, that is a highly alloyed steel (35Fe27Cr31Ni), evaporation of chromium has also been observed in similar environment. However, due to the high Cr/Fe ratio formation of a rapidly growing iron-rich oxide is avoided.(4)

A study published in 2012 compared potassium chloride and potassium carbonate with respect to their tendency to cause corrosion of stainless 304L. Three temperatures were used; 500, 550 and 600 degrees Celsius in both dried air and air consisting of 30% water for 168h. As a reference samples without additional salts were also included in the study. Both salts were found to be corrosive regardless of the surrounding environment, and similarities in the formed oxide were observed. The outermost iron oxide layer followed by a region consisting of chromium, iron and nickel and closest to the bulk material a nickel-rich region appeared. However, the oxide thickness varied between the salts as well as the atmosphere were found to play a significant role when comparing the growth within one type of salt. This may result due to that presence of water at 400 degrees Celsius or above is known to destroy the protective chromium oxide layer without any other corrosive compounds present. For the sample without additional salt exposed in dry air no oxidation was detected, and the formed oxide layer upon the surface were too thin to detect with SEM as well as for EDX analyses. However, the exposure at 600 degrees Celsius in wet condition gave rise to formation of an oxide layer (8-16 μm) enriched with chromium and nickel indicating that the oxide had not lost its protective properties. Depletion of chromium though evaporation, converting the oxide into an iron-rich nonprotective oxide was not detected, which could be due to shorter exposure times or lower water content then used in similar studies reported. (5)

1.2 Aim

In this study the effect of nickel addition on corrosion will be investigated by performing exposures on a set of Fe-base model alloys containing 18 wt% Cr. The exposures will be performed in dry conditions (5% O_2, N_2) in a horizontal tube furnace in 600 ℃ to study the primary protection through mass gain. The aim is to increase the understanding of how addition of nickel influences the primary protection in 18%Cr-containing alloys. This is of great importance since nickel is an expensive alloying element.

1.3 Limitations

This study will not investigate the secondary protection. The analytical work will be limited since this is a mass gain study, and some analysis will only be done on representative samples and/or samples of interest. SEM, EDX and using bare eyes in order to look for differences in colour appearance of the oxides are methods that will be used in various extent. This work is limited to investigate the following alloys: Fe18Cr, Fe18Cr2Ni, Fe18Cr5Ni, Fe18Cr10Ni, Fe18Cr20Ni, Fe18Cr34Ni, 18Cr82Ni.

2
Materials

Metals has a wide range of application areas, each with properties that needs to be considered and prioritized. Due to economic aspects and performance requirements usage of alloys instead of pure metals often are preferred since it both lowers the costs and at the same time retains favoured properties, or even improve them. There are endless amounts of different alloys out on the market, and when choosing one for a specific application life-time and performance along with the price is of major importance, since it could be pricy to invest in an alloy with better properties then necessary. One commonly used type of steel is the stainless steels which will be presented in this chapter.

2.1 Stainless steel

Stainless steels are commonly used iron-based alloys with many application areas, example of application areas are chemical processing industries, power generation, food production as well as for kitchenware, or toolware just to name a few. One reason for the many applications is that stainless steels (12 wt%<Cr<25wt%)(6) classifies as a corrosive resistant material with mechanical preferable properties(6). Stainless steels are divided into groups with respect to their crystal structure. They can either be austenitic, ferritic or martensitic, but also duplex which refers to a mixture of ferritic (40-55%) and austenitic (bal.) structure. Most common is the austinite, with its face-centred cubic structure (FCC), followed by ferrite that has a body-centred cubic structure (BCC). Besides, stainless steels are divided into grades, where the 300-serie (FeCrNi-alloys) is the widest used austenitic steels. In addition to iron, chromium and nickel is two alloying elements added to especially austenitic stainless steels in various amounts. Properties of these elements are discussed more thorough later in this work (see 2.2 Alloying elements). In order to achieve a fully austenitic stainless steel a minimum of 18 wt% Cr and 8 wt% Ni is required while ferritic (α-Fe) steels contain little to no nickel. Austinite (γ-Fe) is most often preferable to use since it is less brittle, have better corrosion resistance, formability and weldability in comparison to ferritic steels. However, depending on the requirements for the specific application an austenitic steel may not be necessary. This makes it interesting to investigate whether greater levels of nickel rise the price more than it contributes to improvement of the properties for the general case. As mentioned, the 300-serie are in general the most common used alloys, where 304L (18-20 wt% Cr, 8-12 mass% Ni) and 347 (18-20 mass%, 8-10,5 mass% Ni) are two examples. (5-6) Another example of a stainless steel, that is more extensively alloyed, is Sanicro 28 (34Fe27Cr31Ni2Mn0.7Si3.5Mo0.02C1.0Cu).(4)

2.2 Alloying elements

Alloying elements are used to a great extent in order to increase properties for specific applications. One reason for adding such elements are to improve the corrosion resistance, mechanical strength but also ductility, malleable, and weldability are properties that improves by the addition. There are plenty of different elements that could be added, each with various outcomes in the aspect of effecting the alloy. As mentioned briefly, nickel and chromium are two elements added to stainless steels. In this subchapter properties of these two elements will be discussed.

2.2.1 Chromium

Chromium is giving rise to the stainless properties in stainless steels due to the formation of chromium rich corundum type oxide scales located on the alloy surface. The oxide acts as a diffusion barrier effecting the oxidation rate, to confer the formation levels above ~13wt% is required. However, the exact chromium content needed to form a protective oxide is still diffuse even though an extensive amount of studies has been carried out over the years, which makes referred values approximate. Modification of the passivating characteristics, along with change in phase equilibria, is possible if other additional elements are introduced.(6) Chromium is also used for improving hardness, wear-resistance and high temperature strength. (8) Figure 1 shows an Fe-Cr phase equilibria where at 600℃ and chromium content below approximately 20% is assigned to a ferritic phase (α-phase), while above 20% Cr the phase shifts from α+σ, to pure σ, and back again to α+σ. (7)

2.2.2 Nickel

Nickel is an important alloying addition in nearly 75% of stainless steels produced today. One primary function is, as mentioned, that it stabilizes the austenitic structure, even at room temperature and below. Nickel is known to lower ductile-to-brittle-transition temperature (DBTT), the temperature below which the alloy becomes brittle. Besides, nickel also contributes with significantly better high temperature strength to alloys. Addition of nickel also promotes the stability of the protective oxide film and reduces spalling during thermal cycling. Consequently, austenitic grades, especially 300-series, are favoured for high temperature applications. The continuum in composition between austenitic stainless steels and nickel-based superalloys used in the most demanding high temperature applications, such as gas turbines. The chromium-rich oxide layer that accounts for the corrosion resistance in stainless steels is susceptible to damage, particularly in presence of chlorides, this type of damage can lead to localised corrosion such as pitting and crevice corrosion. Nickel is for those cases important as it reduces the rate at which these propagates.(9)

In comparison with figure 1, figure 2 also presents an Fe-Cr-phase equilibrium but with addition of 8 mass% Ni. What happens is that the γ-loop widens significantly and thereby also the range for austinite to form in its face-centred-cubic structure (FCC). Note that addition of nickel is not only beneficial since it also leads to an extended sigma phase, meaning that the alloy could lose its ductility, toughness and corrosion resistance. For commercial austenitic steels the balance between maintained performance and minimum cost is a major concern assigned to the nickel content since nickel is one of the most expensive alloying elements.(7)

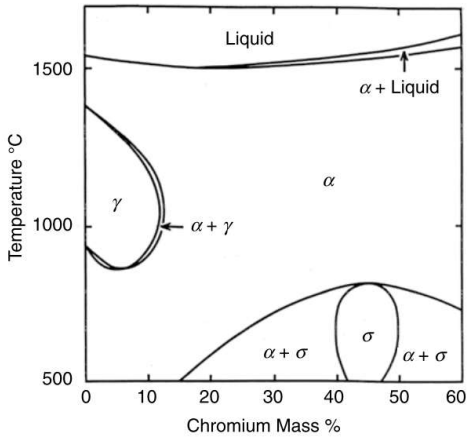

Figure 1 Phase equilibrium of an Fe18Cr alloy (7)

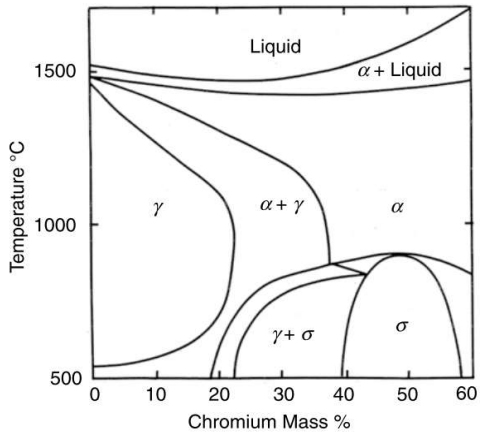

Figure 2 Phase equilibrium of an Fe18Cr8Ni alloy (7)

3
Oxidation of Metals

In presence of oxygen most metals are thermodynamically unstable and thereby react spontaneously with its environment. As the reaction of oxygen and metal proceeds a surface oxide layer starts to form which eventually will limit the contact between the metal and the oxidizing environment. The formed oxide layer may act protective to the substrate metal but could also thicken into a non-protective scale with various defects.
In addition to thermodynamics, knowledge of the kinetics is of major importance to improve the understanding of the oxidation process. In short, thermodynamics state whether oxidation is possible, and kinetics estimates the oxidation rate.

3.1 Thermodynamics

Thermodynamics is one central aspect that need to be taken into consideration when discussing oxide formation. In order to enable spontaneous formation of an oxide the standard Gibbs free-energy, $\Delta G°$, must be negative. Gibbs free-energy could be written as equation 1

$$\Delta G° = \Delta H° - T\Delta S° \qquad \text{(Equation 1)}$$

where $\Delta H°$ is the enthalpy, T temperature and $\Delta S°$ entropy in standard state. When plotting $\Delta G°$ versus temperature an straight line occurs. A collection of various plots of oxidation reactions in standard state has given rise to the diagram known as the Ellingham diagram in Figure 3, where $\Delta H°$ is the axis intercept and $\Delta S°$ is the slope. As mentioned, negative free energy is required in order to receive a spontaneous oxide formation and the lower the oxide reaction are in the diagram the more negative are the standard free energy of formation which corresponds to more stable oxides.(10) The Ellingham diagram could also be helpful when estimating different oxide layers, if more than one forms. The oxides that are considered most stables are also those who will occur closest into the metal.

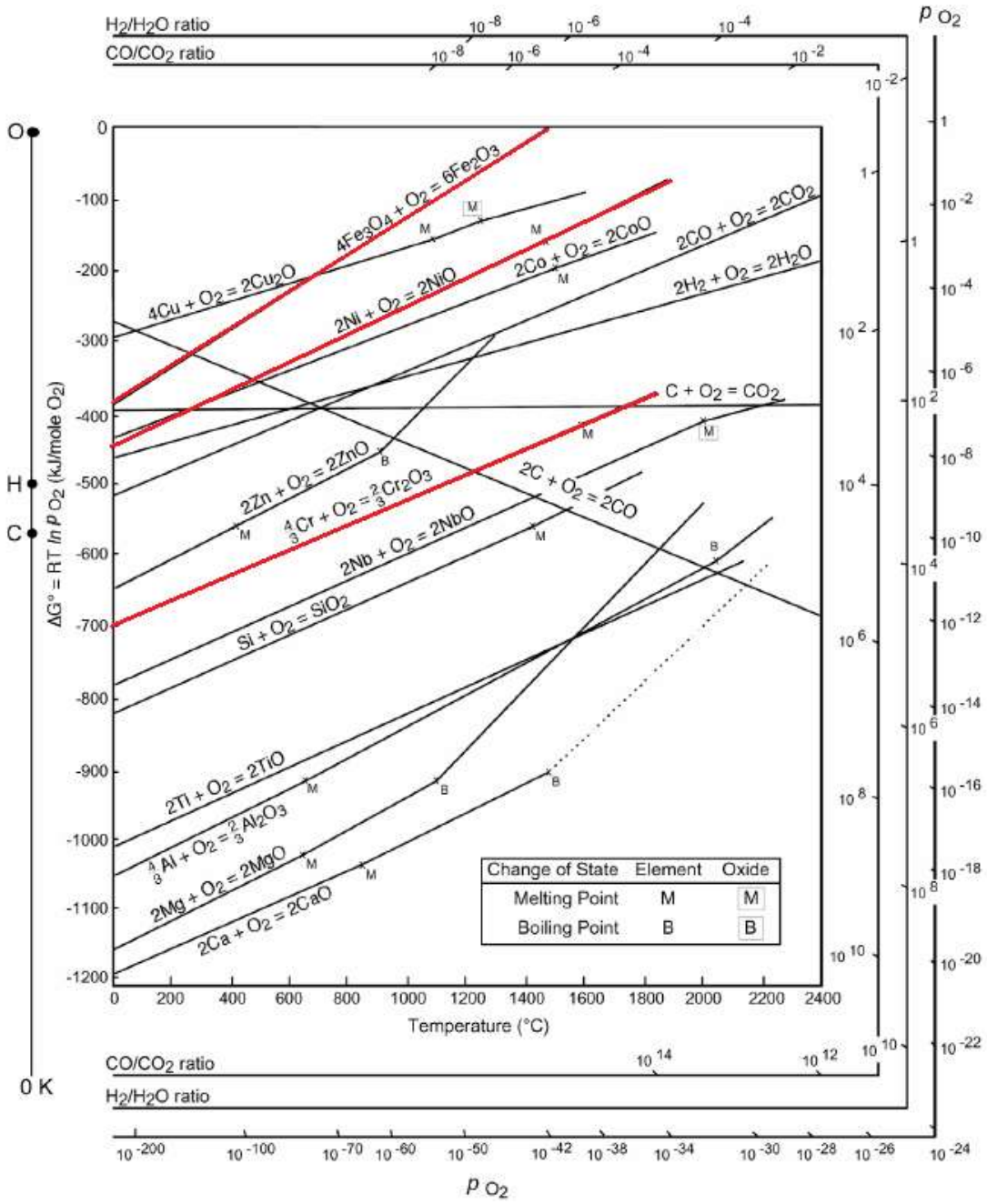

Figure 3 Ellingham diagram from (11) *marked with oxides that may form in this study.*

3.2 Oxide formation

Oxidation proceeds, in general terms, according to reaction 1 below

$$xM + \frac{1}{2}y\ O_2(g) \rightarrow\ M_xO_y(s) \qquad \text{(Reaction 1)}$$

where the metal is written as M, oxygen as O, and x and y are stochiometric constants. Reaction 1 is only valid if it occurs spontaneously which, as mentioned above, requires the free energy to be negative.

Provided that oxidation is possible for the specific case the initial step of the oxide formation is assigned to the metal surface adsorbing oxygen, which further reduces O_2 to O^{2-} ions since the metal liberates electrons that reaches the molecular oxygen, see reaction 2 and figure 4a. The adsorbed oxygen anions then react with the metal cations (M^{n+}) and formation of oxide nuclei begins, as is illustrated in figure 4b. As the growth of the oxide nuclei proceeds over the surface a thin oxide layer starts to form, see figure 4c. Reaction 2 and 3 are electrochemical cathodic and anodic reactions respectively. The transport of ions through the oxide is mandatory in the aspect of further growth. This transport can occur by diffusion through point defects in the crystal lattice, but also by short-circuit diffusion located to grain-boundaries, voids or eventual cracks in the oxide film. (10)

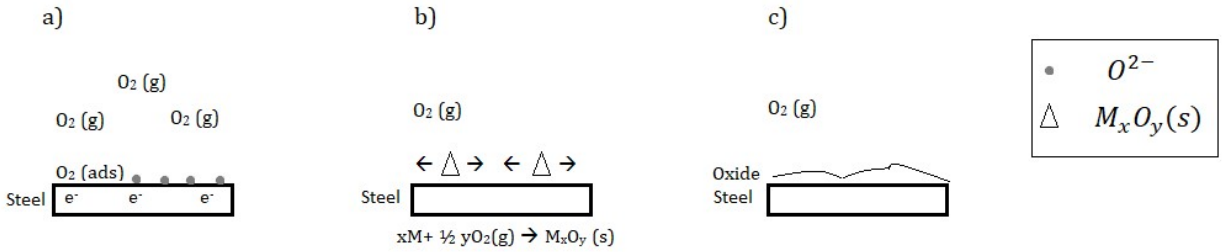

Figure 4 An illustrative picture of a) metal surface adsorbing oxygen and liberating electrons, b) formation of oxide nuclei and c) formation of oxide layer.

$$\frac{1}{2}O_2 + 2e^- \rightarrow O^{2-} \qquad \text{(Reaction 2)}$$

$$M \rightarrow M^{n+} + ne^- \qquad \text{(Reaction 3)}$$

Metal oxides are rarely exactly stoichiometric. Usually they have excess or deficit of metal, equivalent to a deficit and excess of oxygen. For instance, metal-deficit oxides contain M^{2+} cations vacancies which leaves a vacancy of relative charge -2. The diffusion occurs in the lattice where the cations exchange with the cation vacancies. Every cation vacancy is electrically neutralized by a pair of electron “holes”, equivalent to M^{3+} cations having either deficit or excess charge of +1. The electron “hole” exchanges electrons with neighbouring normally charged cations. These types of oxides are referred to as p-type semiconductors and could be seen schematically in figure 5. Metal-excess oxides carries the excess at interstitial cations or oxygen anion vacancies. The interstitial cations jump from one position to another during the diffusion, see figure 6 However, when cations are greater to size then accepted in order to fit or are to highly charge, anions vacancies are required to form the metal-excess structure, see figure 7. These are known as n-type oxides. (10)

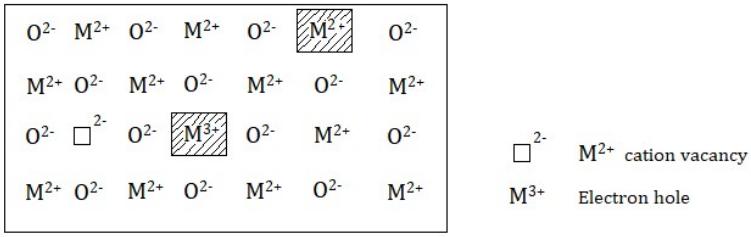

Figure 5 p-type deficit oxide semiconductor with cation vacancies. Created with inspiration from (10).

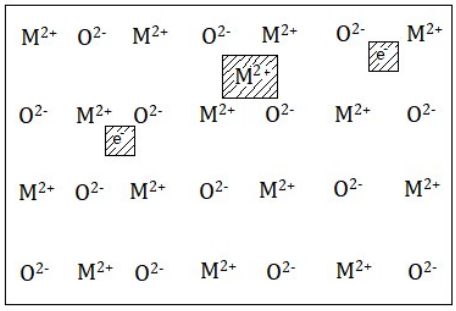

Figure 6 Metal excess n-type metal oxide with free electrones and intersitial metal cations. Created with inspiration from (10).

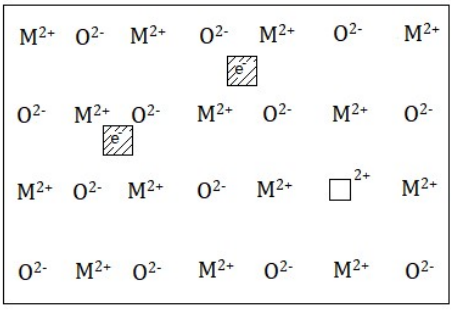

Figure 7 Metal excess n-type oxide with anion vacancies and free electrons. Created with inspiration from (10).

Even though the formation of an oxide is successful, there are some properties that preferably should be fulfilled. Some of the favoured properties are listed below and are cited from (10)

1. The film should have good adherence, to prevent flaking and spalling.
2. The melting point of the oxide should be high.
3. The oxide should have low vapour pressure to resist evaporation.
4. The oxide film and metal should have close to the same thermal expansion coefficients.
5. The film should have high temperature plasticity to accommodate differences in specific volumes of oxide and parent metal and differences in thermal expansion
6. The film should have low electrical conductivity and low diffusion coefficients for metal ions and oxygen.

Beside the listed properties the film should preferably be continuous and relatively slow growing.

3.3 Oxidation kinetics

When discussing oxidation kinetics of metals there are three kinetic rate laws – linear, parabolic, and logarithmic- referred to as ideal cases, which together describes the oxidation rates for most metals and alloys. The appearance of the different rate laws, and breakaway, presented in weight gain versus time could be seen in Figure 8 below. Knowledge of the oxidation kinetics is important in the aspect of understanding the behaviour of which the oxidation process follows and is a good tool when predicting approximate oxide formation for a certain alloy.

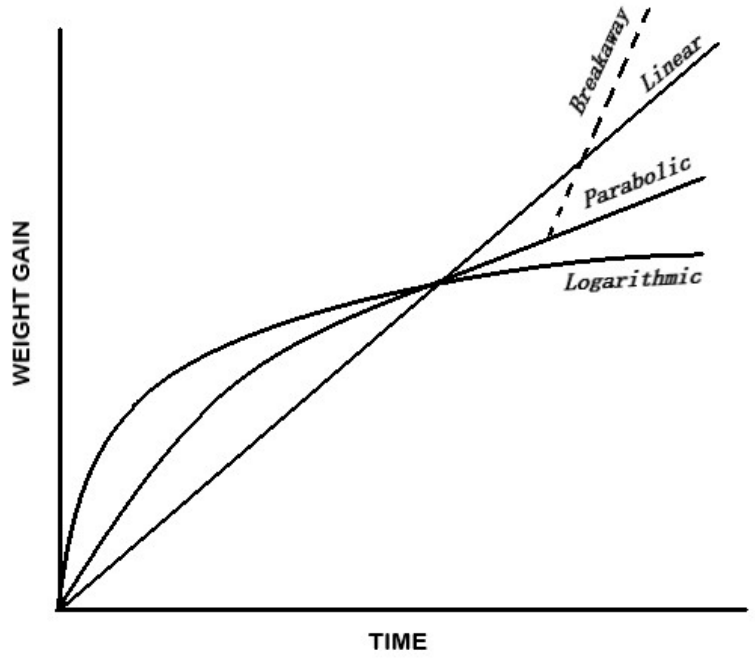

Figure 8 Weight gain versus time for the parabolic, linear, and logarithmic kinetic laws along with breakaway. Created with inspiration from (10).

3.3.1 Linear rate law

In those cases where the oxidation rate is constant over time, independent of the amount of gas or metal consumed, the linear rate law is applicable, written as equation 2 or equation 3.

$$\frac{dx}{dt} = K_l t \qquad \text{(Equation 2)}$$

$$x = K_l t + C \qquad \text{(Equation 3)}$$

where K_l is the linear rate constant, t time, x oxide thickness and C the integration constant. (12) A linear law may result when a reaction at a phase boundary controls, provided that the eventual surface film is non-protective, meaning that the substrate metal has access to the oxidizing gas. (10)

3.3.2 Parabolic rate law

In high temperature corrosion metals most often follows the parabolic rate law, which requires the square of the oxide thickness to be proportional to time, seen as equation 4.

$$x^2 = k_p t + C \qquad \text{(Equation 4)}$$

k_p is the parabolic rate constant, t time and x corresponds to the film thickness. The parabolic growth has earlier been explained by Wagner who assumed that the oxide is compact and utterly adherent and that ion migration through the oxide is rate controlling. (10)

3.3.3 Logarithmic rate law

The direct logarithmic, and inverse logarithmic rate law represent oxidation in thin layer regimes and is for most metals valid when heated at low temperatures. Equation 5 and 6 represents the direct and inverse logarithmic rate law respectively.

$$x = k \log (t + t_0) + C \qquad \text{(Equation 5)}$$

$$\frac{1}{x} = B + K' \log t \qquad \text{(Equation 6)}$$

x corresponds to the oxide thickness, t denotes time, K and K´ are rate constants, A and B are the integration constants. (12)

3.3.4 Breakaway oxidation

Breakaway oxidation occurs when the once protective oxide layer degrades due to reaction with the environment, or if it suffers from cracks or other defects. As could be seen in figure 8, breakaway causes an accelerating weight gain in comparison with the three other oxidation rate laws mentioned, indicating that a more fast-growing oxide most likely starts to form.

4
Corrosion Products

Metals are most often unstable in presence of oxygen, which leads to formation of oxides. These could be either slow- or fast growing, be protective or non-protective. Dependent on the composition of an alloy, the surrounding environment and temperature different types of oxides forms. By using an Ellingham diagram if these parameters are known, a good estimation could be done regarding which oxide most likely will be formed. For dry oxidation there are five oxides in the iron-chromium-oxygen system, FeO (wüstite), Fe_3O_4 (magnetite), Fe_2O_3 (haematite), Cr_2O_3 and $FeCr_2O_4$ (chromite). When presence of high amounts of nickel, also nickel-rich oxides can form. In this chapter some different oxides will be presented.

4.1 Chromium oxides

In the iron-chromium-oxygen system chromium could form Cr_2O_3 and $FeCr_2O_4$ (chromite), but also a mixed oxide together with Fe_2O_3 as $(Fe, Cr)_2\ O_3$ and with $Fe_3\ O_4$ the mixed spinel, $Fe^{II}(Fe,Cr)_2{}^{III}O_4$. However, in FeO the solubility is low. (6)

Chromium oxide, Cr_2O_3, forms a green corundum-type oxide with a hexagonal crystal structure.(13) Besides, Cr_2O_3 is the only stable chromium oxide at high temperature. As mentioned, chromium oxide is considered to act protective for stainless steels in high temperature applications. It has a good corrosion resistance and excellent hardness and does not react to most acids and alkalis. However, exposing chromia forming alloys to some alkalis could cause breakdown, which is done for instance when studying the secondary protection. (14) The lattice transport is sluggish which is one explanation for the good protective properties. The dominant defect for chromium oxides is cation vacancies, making it a p-type conductor. (15) It has been shown that chromia grown on pure chromium can exhibit both n-type and p-type conductivity, controlled by the p(O2), where high p(O2) corresponds to the formation of p-type. The highest p(O2) is located close to the surface. (16)

Chromia could lose its protectiveness if water vapour and/or salts are present. Regardless of process that depletes the oxide it has been observed to suffers from an accelerated corrosion effect. (17)

4.2 Iron oxides

Hematite

Fe_2O_3 also possesses corondum type structure, like Cr_2O_3, which in turn enables formation of the mixed oxide $(Fe, Cr)_2\ O_3$. Oxygen ions are hexagonally closed-packed while Fe^{3+} ions are situated in 2/3 of the octahedral sites of the oxygen lattice. Hematite is considered as an n-type conductor, with both metal interstitials and oxygen vacancies. In spite of that, lattice transport is considered as both outward diffusion of metal cations and inward diffusion of oxygen anions. (15)

Magnetite

Fe3O4 has an inverse spinel structure, with Fe2+ ions and half of the Fe3+ ions filling up the octahedral sites, remaining Fe3+ ions occupy tetrahedral sites. It grows primarily by outward transport of metal ions, and is considered as a p-type semiconductor. (15)

Wüstite

Wüstite, $Fe_{1-y}O$, is only stable at temperatures above 570℃ and at low oxygen activities. It is metal deficient and therefore a p-type semiconductor. The crystal structure consists of oxygen ions that are cubically closed-packed and iron ions located in the octahedral interstices. Wüstite is a complex non-stochiometric oxide with a high diffusion coefficient, resulting in rapid growth of a thick oxide scale. (18)

4.3 Nickel oxides

Nickel oxide, NiO, is a non-stoichiometric semiconductor of p-type. The growth rate of NiO follows parabolic behaviour in presence of water. (19) NiO is ordered in rock salt structure with Nickel and oxygen ions at the octahedral sites.

5
Experimental Procedure

In this chapter the investigated materials are presented along with descriptions of the different stages included in the experimental part of this work.

5.1 Investigated materials

This study is based on a set of mainly Fe18Cr alloys with addition of various amounts of nickel as is presented in Table 1 below. As mentioned in the material chapter in this work austenitic stainless steels requires a minimum of 18wt% Cr and 8wt% Ni, making some of the samples austenitic while some is ferritic or a mixture. The investigated samples are provided as coupons with approx. dimensions of 11x11x2 mm before grinding them. All sample also had a small hole located near one of the edges. All samples were handled likewise throughout the whole experimental procedure.

Table 1 Investigated samples with varying amounts of nickel and iron, and 18wt% Cr.

Matrix of alloys in weight%			
Fe	Cr	Ni	Al
Bal.	18	0	*
Bal.	18	2	*
Bal.	18	5	*
Bal.	18	10	(0.005)
Bal.	18	20	*
Bal.	18	34	*
-	18	82	*

*<0.01

5.2 Sample preparation

The initial step of sample preparation is assigned to grinding and polishing the coupons. Four coupons of each alloy were ground with SiC paper (500 to 4000 grit) followed by polishing with diamond suspension (3 μm and 1 μm) in order to receive a mirror-like surface. Table 2 shows all grinding and polishing steps more thorough. To remove dirt and grease from the polished samples they were placed in separate tubes filled with acetone and further put into an ultrasonic bath. The samples were then cleaned with ethanol to remove eventual acetone remains. Samples were then stored in plastic holders until exposed.

Prior to exposure, all samples were weighted, and dimensions were measured in order to collect data for later calculations on mass-gain and oxide-thicknesses.

Table 2 Grinding and polishing steps of samples.

Grind number	Grinding time [s]	Grinding paper	Grinding liquid
1	40	Silicon carbide grinding paper, grit 500	Distilled water
2	40	Silicon carbide grinding paper, grit 1000	Distilled water
3	35	Silicon carbide grinding paper, grit 2400	Distilled water
4	35	Silicon carbide grinding paper, grit 4000	Distilled water
5	30	MD-Dac	Diamond suspension, 3 μm
6	25	MD-Nap	Diamond suspension, 1 μm

5.3 Furnace exposure

All exposures were carried out in a horizontal tube furnace in 600℃ in dry condition (5% O_2, N_2 (bal.)). The furnace was equipped with a silica tube with an inner diameter of 45 mm connected to multiple gas-pipes. Total gas-flow in this study was 1000 ml/min, and the O_2-source in this case was from air ($\sim 20\%\ O_2$), making the air-flow 250 ml/min and N_2- flow 750 ml/min. To confirm the flow-rates a flowmeter was used. Temperature were measured in the middle of the furnace since samples were located there during exposure.

An alumina plate with three slits were used for all exposures, making it possible to expose three samples at a time. In this study three samples of the same alloy were exposed simultaneously. The alumina plate was inserted carefully, with help of a metal stick, to avoid samples from falling off until it reached the middle of the furnace. After inserting the samples, the furnace was closed, and gas-flows turned on. The furnace was connected to a beaker filled with distilled water, which by the appearance of bubbles confirmed the gas-flow. All samples were exposed for 168 hours, with exception for the first controlling exposure that lasted for 24 hours.

After exposure samples were left to cool for at least one hour before weighing. As the new weights were noted, mass-gain was calculated and further also oxide thicknesses.

5.4 Calculation of oxide thickness

The estimated oxide thicknesses of the oxides were calculated from mass-gain data. The calculation assumes that the mass-gain is assigned to the ingress of oxygen, resulting in the usage of density in order to translate the mass-gain into a volume and further also into oxide thickness. Since the density of the oxide does not only correspond to the oxygen content, a factor is used in order to compensate. The theoretical density change could be written as equation 7.

$$\Delta\rho_{\text{theoretically}} = \rho_{M_xO_y} * \frac{M\,(O_2)}{M(M_xO_y)} \qquad \text{(Equation 7)}$$

where $\rho_{M_xO_y}$ is density for the formed oxide, $M\,(O_2)$ molar mass for oxygen gas, and $M(M_xO_y)$ molar mass for the oxide. Since density is defined according to equation 8

$$\rho = \frac{m}{V} \qquad \text{(Equation 8)}$$

where m in this case corresponds to mass-gain (g/cm^2) and V to arbitrary volume of the oxide. Combining equation 7 and 8, results in equation 9

$$V\,[cm^3] = d\ cm * 1\ cm^2 = \frac{m}{\rho_{M_xO_y} * \frac{M\,(O_2)}{M(M_xO_y)}} \qquad \text{(Equation 9)}$$

where d is oxide thickness. Equation 9 could be re-written as equation 10, receiving the oxide thickness in µm.

$$d = \frac{m}{\rho_{M_xO_y} * \frac{M\,(O_2)}{M(M_xO_y)}} * 10000 \qquad \text{(Equation 10)}$$

6
Analytical Techniques

The analytical methods used in this work is SEM and EDX. With help from the analytical work, estimations regarding formed oxides could be made. The analytical work was performed in company with a supervisor.

6.1 Scanning electron microscopy (SEM)

Scanning electron microscopy uses a focused beam of high-energy electrons in order to generate signals from solid samples surfaces. Signals achieved by the electron-sample interaction, combined with other techniques such as Energy Dispersive X-ray Spectroscopy (EDX), provides information regarding the morphology, chemical composition, and crystalline structure.

Accelerated electrons carry significant amount of kinetic energy which further, when dissipated, result in various signals as the incident electron interacts with the sample. These signals include secondary electrons, backscattered electrons, diffracted backscattered electrons, photons(X-ray) and heat. The X-rays are used in EDX to study the chemical composition of the sample. When imaging samples secondary electrons and backscattered electrons are most commonly used, where the secondary electrons reveal morphology while the backscattered electrons give rise to the contrast assigned to the differences in composition or density. SEM is performed under vacuum and can be used in most cases when examining solid samples, however for instance sample size and detection of light elements (atomic numbers 11>) could be limiting factors. (20)

6.2 Energy Dispersive X-ray Spectroscopy (EDX)

EDX is an X-ray technique used for identification of elemental composition of materials used together with SEM. Data generated from EDX is presented as a spectrum with peaks of different heights where each peak is unique for one element and the higher the peak appears, the greater is the quantity of the detected element. Also, it is possible to do elemental mapping when using EDX. The interaction volume plays a significant role when using this technique since the traced signals is based on all the information provided, which is determined in respect to this volume. For instance, when analysing thin oxides the interaction volume is of major concern since the composition of the steel may be detected if the interaction volume is to extensive. (21)

7
Results

7.1 Influence of nickel

7.1.1 Mass-gain and oxide thickness

Figure 9 shows mass-gain after exposure for 168 hours in 600 ℃ in dry condition (5% O_2, 75% N_2). For alloys containing 0 to 10 wt% Ni the mass-gain is relatively low in comparison to the others, where the 2 wt% Ni alloy had the highest mass gain within this range. For alloys with higher nickel content the mass-gain increased significantly. The highest mass-gain was assigned to the 34 wt% Ni alloy. The colour appearance of the alloys after the exposure matched well with the mass-gain data since the exposed alloys with low mass-gain retained their shiny surface, while those with higher mass-gain received a more matte surface. For the estimated oxide thickness calculations mean-values of the mass-gain was used, presented in Table 3.

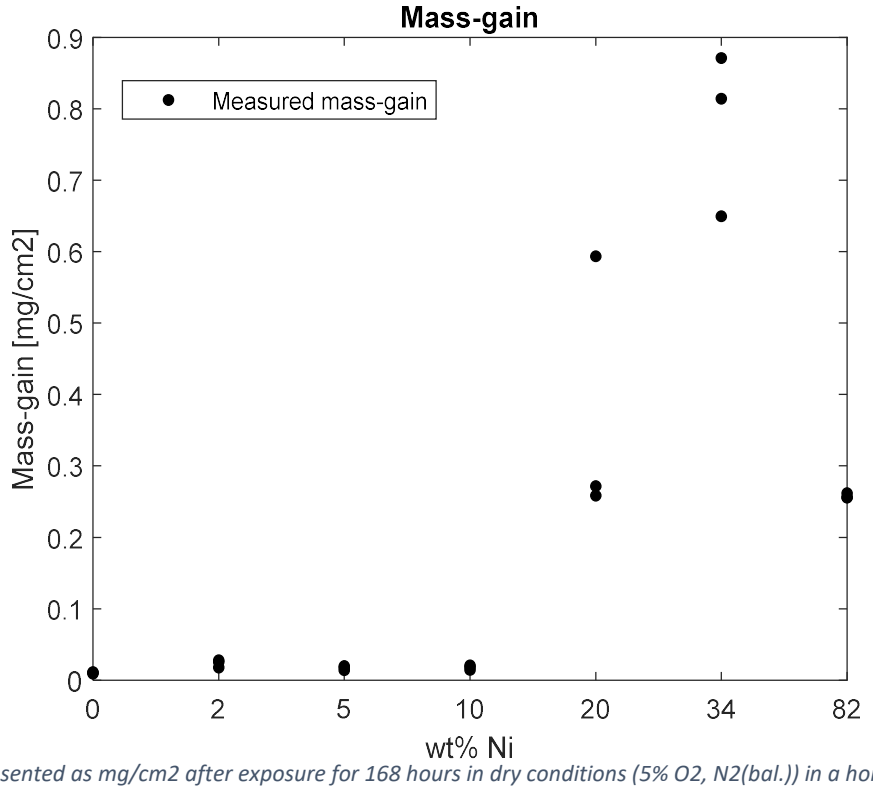

Figure 9 Mass-gain results presented as mg/cm2 after exposure for 168 hours in dry conditions (5% O2, N2(bal.)) in a horizontal tube furnace at 600℃.

Table 3 Average mass-gain results for all alloys.

Alloy	Average mass-gain [mg/cm2]
Fe18Cr0Ni	0,010355102
Fe18Cr2Ni	0,02363247
Fe18Cr5Ni	0,017128927
Fe18Cr10Ni	0,017746331
Fe18Cr20Ni	0,374477329
Fe18Cr34Ni	0,77823962
18Cr82Ni	0,257822259

Mass-gain results after 24 hours of exposure are presented in Figure 10. Results are taken from the TEAMWORK report and is not achieved from this study. The alloy setup is identical.

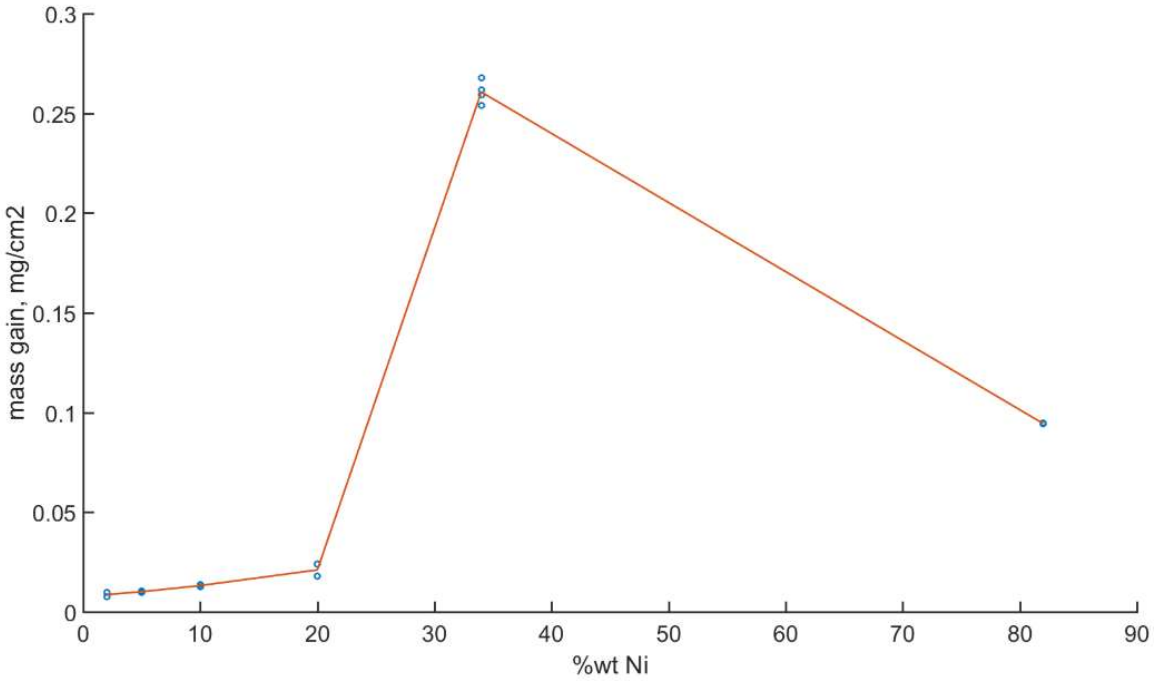

Figure 10 Mass-gain data after exposure in a horizontal tube furnace in 600 degrees Celsius for 24 hours in dry condition (5% O_2, N_2). Results are taken from the TEAMWORK report.

By using the mass-gain data and surface area of the coupons a theoretical oxide thickness was calculated and results are presented in Table 4. Since density of formed oxide is part of the equation used when calculating the theoretical oxide thickness assumptions are needed.

Table 4 Calculated oxide thicknesses for all alloys with estimated oxide formed, given in nanometres.

Alloy	Oxide thickness (nm)	Estimated oxide formed
Fe18Cr	96	Cr_2O_3
Fe18Cr2Ni	232	Cr_2O_3
Fe18Cr5Ni	159	Cr_2O_3
Fe18Cr10Ni	166	Cr_2O_3
Fe18Cr20Ni	2471	Cr_2O_3/Fe_3O_4
Fe18Cr34Ni	7509	Fe_3O_4
Fe18Cr82Ni	1823	NiO

7.1.2 Analytical results

Analytical results for this study are presented as plan-view SEM images of the different alloys with varying magnifications and EDX analysis.

7.1.2.1 Colour appearance

Pictures of all samples are presented in Figure 11 a-i below. Alloys consisting of 0-10% Ni (see Figure 11 a-d) remained their shiny surface after the furnace exposure, while alloys with 34 and 82 % Ni (see Figure11 g-i) turned matte. However, samples consisting of 20%Ni (see Figure 11 e-f) showed one side that remained shiny, while the other side were predominantly matte. The 82%Ni showed a matte surface, while the edges had a shiny blue appearance similar to the surface of the 0%Ni. As could be noted the 2 and 5%Ni alloys look similar with their gold-like colour even though the oxide thickness were greater for the 2 Ni alloy. The 10%Ni alloy showed a mixture of gold-like and blue colour appearance. The alloy consisting of 20%Ni showed two shiny surfaces, with one covered by matte reddish spots spread homogenously on the sample surface. The 34%Ni appeared with a matte greyish colour with red spots located mainly on the edges of the surface. The increase of nickel mainly changed the surface from shiny to matte, which overall correlate well with the mass-gain results, as the alloys with high mass-gains tended to be more matte.

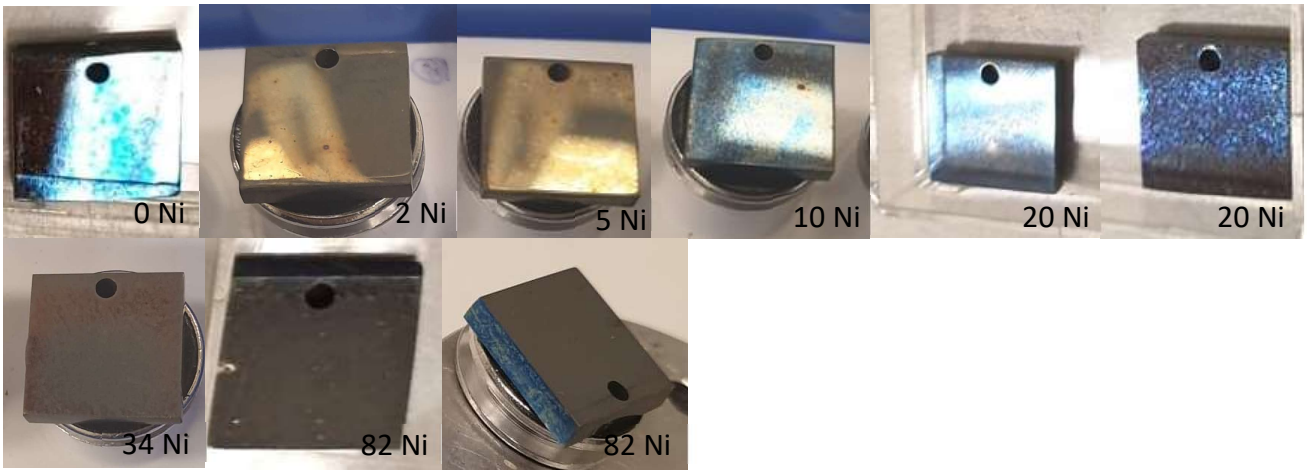

Figure 18 Pictures of Fe18Cr, Fe18Cr2Ni, Fe18Cr5Ni, Fe18Cr10Ni, Fe18Cr20Ni, Fe18Cr34Ni and 18Cr82Ni after 168 hour exposure.

7.1.2.2 Scanning Electron Microscopy (SEM) and EDX-analysis

All samples were imaged for magnification 50, 200, 400, 800, 1600, and 3000x. However, some of the samples had additional magnifications imaged. Figure 12-18 show SEM images of all exposed alloys at magnification 800x since the differences between the alloys could easily be observed. Some surfaces appeared as rather smooth in comparison with those with more extensive oxide growth. Mass-gain results indicated that as the nickel content increased a higher mass-gain was observed. However, the highest mass-gain was assigned to the 34%Ni alloy which also received the thickest estimated oxide thickness. As could be seen in Figure 12 and Figure 15, the 0% Ni and 10% Ni had smoother surfaces than the other alloys. While for the 2% Ni, 5% Ni, 20% Ni and 34% Ni oxides are easier to distinguish as the nickel content increases, and the appearance of different regions could more easily be observed. However, at higher magnifications the metal grains get more prominent for the

0%Ni and 10%Ni alloys, even though the observed differences are insignificantly small. Since the alloys with 10%Ni or less formed thin oxides the metal grains observed does indicate that the interaction volume is deeper than the thickness of the oxide. The 82%Ni alloy had an outstanding appearance in comparison to the other alloys, which most likely is due to the fact that only trace levels of iron are present. As could be seen in Figure 18 the oxide growth is more extensive in the grains rather than in the grain boundaries and a more even oxide profile is observed in comparison to the other alloys.

The EDX analysis was useful in order to estimate what type of oxides that have formed on the different alloys. For the alloys containing 0 to 10 wt% Ni a thin and chromium-rich oxide, Cr_2O_3, most likely formed based on the detected signals from the EDX analysis but also the shiny surface indicated that the sample remained. The surface of the alloy containing 20 wt% Ni was partly covered by a thin Cr-rich oxide, but also showed regions with thicker Fe-rich oxides (see Figure 16). For the 34 wt% Ni, EDX analysis indicated that an iron-rich oxide formed all over the sample surface except for in the alloy grain boundaries. For the 82 wt% Ni alloy a Ni-rich oxide were predicted to form assigned to the predominant Ni-content. The results achieved from the EDX analysis correlated well with this estimated outcome. However, in Figure 18 the grain boundaries are notably brighter than the rest of the sample surface, which most likely is due to the formation of a thinner oxide. Results from the EDX analysis indicated that the grain boundaries had significantly higher chromium concentrations than the rest of the sample which could explain this appearance.

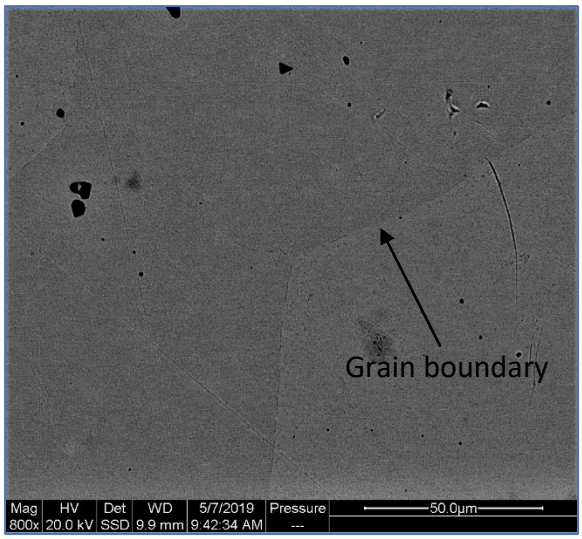

Figure 12 Plan-view SEM image of 0Ni

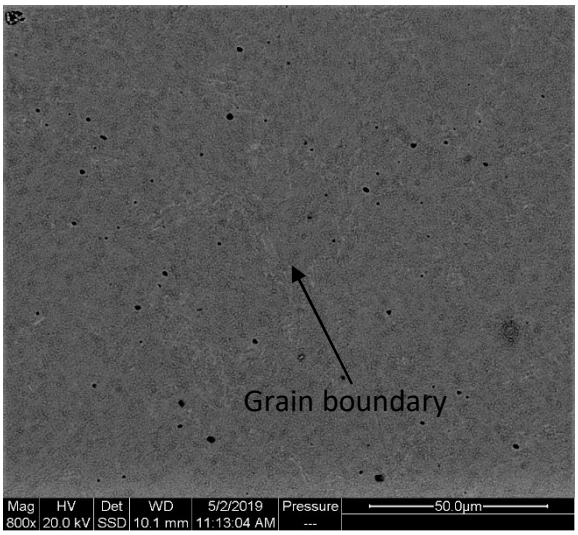

Figure 13 Plan-view SEM image 2Ni

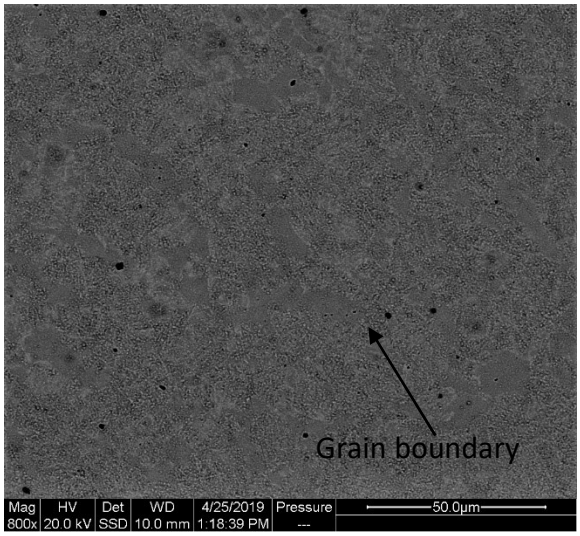

Figure 14 Plan-view SEM image 5 Ni

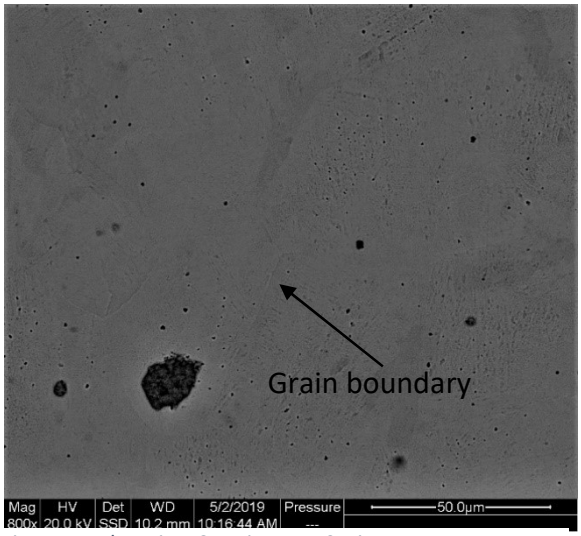

Figure 15 Plan-view SEM image 10 Ni

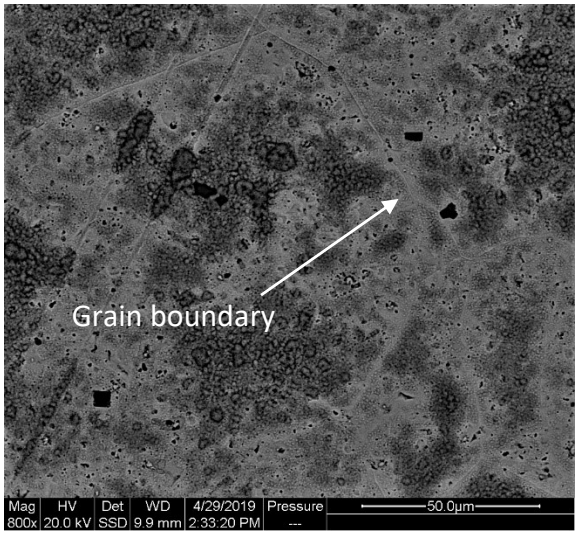

Figure 16 Plan-view SEM image 20 Ni

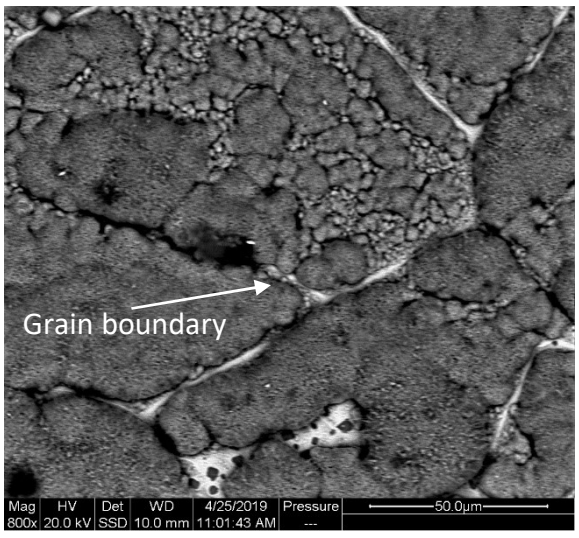

Figure 17 Plan-view SEM image 34 Ni

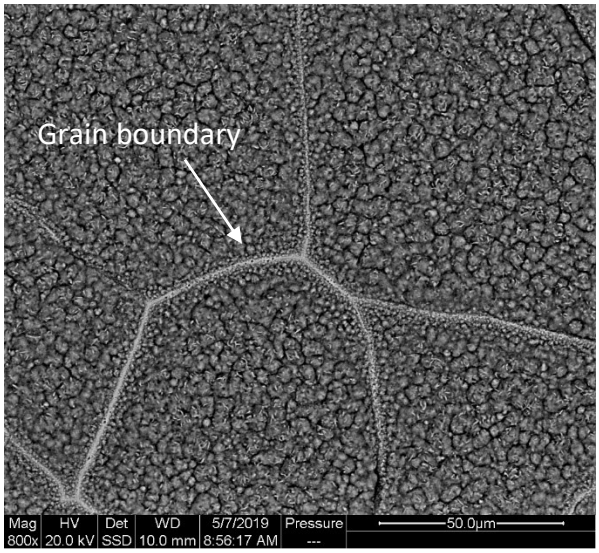

Figure 18 Plan-view SEM image 82 Ni

8
Discussion

Out of this study it could be stated that something happens for the FeCr-alloys consisting of 20 wt% Ni or higher. Differences between the samples could be observed as soon as they were taken out of the furnace since the colour appearance differed. However, mass-gain data and EDX results were necessary to point out the differences more specificaly. In general, alloys consisting of 20wt% Ni or higher appeared with a matte surface and had the highest mass-gains, while the alloys with less Ni had a shinier appearance and lower mass-gain. When comparing results between this work and the TEAMWORK project, it was noted that the 20wt% Ni alloy was more similar in growth as the ones with lower Ni content, which was not the case for this study. The only parameter that differed between these two works is exposure time, indicating that the exposure time is of importance for the outcome seen to mass-gain.

EDX-analysis generally showed differences in the composition between the brighter and darker regions, were the darker regions most likely corresponded to an initial formation of iron-rich oxide. Alloys consisting of 20wt% Ni or higher had mostly dark regions, and also the highest mass-gain which correlates well with this conclusion.

Looking at the 304L study presented earlier in this work it was concluded that regardless of the surrounding environment, wet or dry, both salts (?+?) acted corrosive and the outermost oxide layer consisted of iron oxide. Potassium carbonate salt (K_2CO_3) were also used in a study executed on the same batch of alloys as in this work, exposed in the exact same way but focused on the secondary protection(22). Here iron rich oxides formed, after breakdown of the primary protection, as well as nickel oxide for the alloy that only consisted of trace levels of iron.

The secondary protection study used 1 mg/cm2 K_2CO_3 to cause breakdown of the primary protection. Alloys were treated in the same way as in this work, except from the added salt, but results differed notably. Low nickel content alloys, with less than 5 wt% Ni, had the highest mass-gains, while the once with higher amounts of nickel had low mass-gain. From TG – and furnace exposures it was noted that the Fe18Cr5Ni nickel addition increases the primary – and secondary protection properties. As the primary protection held longer when salt was added, and the alloy had a decreased mass-gain after breakaway. For alloys consisting of more than 5 wt% Ni the primary protection fails immediately which forces the secondary protection to form. One parameter that may have influence in this case is the Cr/Fe ratio.

Since metals are used in a wide range of applications, in varying environments, the comparison between these two works show that if a metal are thought to be used in a alkaline environment, including breakdown corrosion, alloys with higher nickel content most likely will be the better option. However, this study indicates that if the application is in a mild and clean environment, nickel addition above 20% appear to have a detrimental effect at a chromium content of 18 wt%, possibly due to the relatively low Cr/Ni ratio.

9
Future work

This study showed that the mass-gain increased notably for Fe18Cr20Ni and Fe18Cr34Ni, making it interesting to limit a future work to more similar compositions but also perform a better kinetic study to easier follow the mass-gain continuously. Implementing longer exposure times with the same alloys under the same conditions as for this work would also be interesting since there is a notable change in mass-gain for the 20 wt% Ni alloy between 24- and 168-hour exposures.

Also, using the same nickel content as for this study but varying the composition of chromium (chaging the Cr/Ni ratio) would have been of interest to look at since the formation of chromium rich oxide is of importance for stainless steels.

Except for adding salt, also water is also known to cause breakaway corrosion of chromia forming alloys, thereby it would be interesting to see what influence process steam or likewise would have on the alloys with higher amounts of Ni.

Bibliography

1. Stainless steel : The role of nickel [Internet]. Nickel Institute. [cited 2019 May 24]. Available from: https://www.nickelinstitute.org/about-nickel/stainless-steel/
2. Khan MA, Sundarrajan S, Natarajan S, Parameswaran P, Mohandas E. Oxidation and Hot Corrosion Behavior of Nickel-Based Superalloy for Gas Turbine Applications. Mater Manuf Process [Internet]. 2014 Jul;29(7):832–9. Available from: http://10.0.4.56/10426914.2014.901530
3. Asteman H, Svensson J-E, Johansson L-G, Norell M. Indication of Chromium Oxide Hydroxide Evaporation During Oxidation of 304L at 873 K in the Presence of 10% Water Vapor. Oxid Met [Internet]. 1999 Aug;521.(1):95–111. Available from: https://doi.org/10.1023/A:1018875024306
4. Pettersson C, Jonsson T, Proff C, Halvarsson M, Svensson J-E, Johansson L-G. High Temperature Oxidation of the Austenitic (35Fe27Cr31Ni) Alloy Sanicro 28 in O2 + H2O Environment. Oxid Met [Internet]. 2010 Aug;74(1):93–111. Available from: https://doi.org/10.1007/s11085-010-9199-1
5. Lehmusto J, Skrifvars BJ, Yrjas P, Hupa M. Comparison of potassium chloride and potassium carbonate with respect to their tendency to cause high temperature corrosion of stainless 304L steel. Sience Direct [Internet]. 2013;105:98–105. Available from: http://resolver.ebscohost.com/openurl?sid=EBSCO%3Aedselp&genre=article&issn=03783820&ISBN=&volume=105&issue=&date=20130101&spage=98&pages=98-105&title=Fuel+Processing+Technology&atitle=Comparison+of+potassium+chloride+and+potassium+carbonate+with+respect+to+their+tendency+to+cause+high+temperature+corrosion+of+stainless+304L+steel&aulast=Lehmusto%2C+J.&id=DOI%3A10.1016%2Fj.fuproc.2011.12.016&site=ftf-live
6. Talbot, David E.J.Talbot JDR. Corrosion Science and Technology (3rd Edition) - Knovel [Internet]. 2018 [cited 2019 Apr 10]. Available from: https://app.knovel.com/web/toc.v/cid:kpCSTE0001/viewerType:toc//root_slug:corrosion-science-technology/url_slug:iron-chromium-system?=undefined&issue_id=kt011MIIK9&hierarchy=kt011MIIJ8%2Bkt011MIIK9
7. Elbakhshwan MS, Gill SK, Rumaiz AK, Bai J, Ghose S, Rebak RB, et al. High-temperature oxidation of advanced FeCrNi alloy in steam environments. Appl Surf Sci [Internet]. 2017 Dec 31 [cited 2019 May 7];426:562–71. Available from: https://www.sciencedirect.com/science/article/pii/S0169433217319736
8. Downing JH, Bacon FE. Chomium processing. In: Encyclopaedia Britannica [Internet]. Encyclopaedia Britannica, inc; 2013 [cited 2019 May 14]. Available from: https://www.britannica.com/technology/chromium-processing
9. The nickel advantage [Internet]. Nickel Institute. [cited 2019 May 22]. Available from: https://www.nickelinstitute.org/about-nickel/stainless-steel/the-nickel-advantage/
10. Jones DA. Principles and Prevention of Corrosion. Second edi. Prentice Hall: EBSCOhost; 1996.
11. Ellingham diagram [Internet]. The National Energy Technology Laboratory of the U.S Department of Energy. [cited 2019 May 27]. Available from: https://www.netl.doe.gov/sites/default/files/ event-proceedings/fuel-cells-

archive/IC-Pitt-Meier-Extras.pdf
12. Khanna AS. Introduction to high temperature oxidation and corrosion [internet]. ASM International; 2002.
13. Zhao P, Zhao H, Yu J, Zhang H, Gao H, Chen Q. Crystal structure and properties of Al2O3-Cr2O3 solid solutions with different Cr2O3 contents. Ceram Int [Internet]. 2018 Feb 1 [cited 2019 May 20];44(2):1356–61. Available from: https://www.sciencedirect.com/science/article/pii/S0272884217318709
14. Zamani P, Valefi Z. Microstructure, phase composition and mechanical properties of plasma sprayed Al2O3, Cr2O3 and Cr2O3-Al2O3 composite coatings. Surf Coatings Technol [Internet]. 2017 Apr 25 [cited 2019 May 20];316:138–45. Available from: https://www.sciencedirect.com/science/article/pii/S025789721730261X
15. Tang JE. The influence of water vapour on the oxidation behaviour of high-temperature materials : microstructure investigation using analytical electron microscopy. [Internet]. Chalmers tekniska högsk.; 2004. (Doktorsavhandlingar vid Chalmers tekniska högskola: Ny serie 2092). Available from: http://proxy.lib.chalmers.se/login?url=http://search.ebscohost.com/login.aspx?direct=true&db=cat06296a&AN=clc.b1292608&site=eds-live&scope=site
16. Latu-Romain L, Parsa Y, Mathieu S, Vilasi M, Galerie A, Wouters Y. Towards the growth of stoichiometric chromia on pure chromium by the control of temperature and oxygen partial pressure. Corros Sci [Internet]. 2017 Sep 1 [cited 2019 May 20];126:238–46. Available from: https://www.sciencedirect.com/science/article/pii/S0010938X17302457
17. Pettersson J, Folkeson N, Johansson L-G, Svensson J-E. The Effects of KCl, K2SO4 and K2CO3 on the High Temperature Corrosion of a 304-Type Austenitic Stainless Steel. Oxid Met [Internet]. 2011 Aug;76(1):93–109. Available from: https://doi.org/10.1007/s11085-011-9240-z
18. Eklund J. Material Solutions for Mitigating High Temperature Corrosion in Biomass-and Waste-fired Boilers. Chalmers university of technology, Gothenburg, Sweden; 2018.
19. Jonsson T, Slomian A, Lomholt TN, Kiamehr S, Dahl K V. Microstructural investigations of pure nickel exposed to KCl induced high temperature corrosion. Mater High Temp [Internet]. 2015 Jan 1;32(1–2):44–9. Available from: https://doi.org/10.1179/0960340914Z.00000000060
20. Swapp S. Scanning Electron Microscopy (SEM) [Internet]. [cited 2019 Jun 16]. Available from: https://serc.carleton.edu/research_education/geochemsheets/techniques/SEM.html
21. Energy Dispersive X-ray Analysis (EDX) [Internet]. Intertek. [cited 2019 Jun 16]. Available from: http://www.intertek.com/analysis/microscopy/edx/
22. Fung W. The influence of Ni on corrosion of Fe18Cr model alloys at 600 °C. Chalmers University of Technology, Gothenburg,Sweden; 2019.